DESIGNING EXPERIMENTS TO ASSESS THE SPACE-TIME DYNAMICS OF PLANT DISEASES

A Thesis

Presented to

The Faculty of Graduate Studies

of

The University of Guelph

by

DARIA MARTCHENKO

In partial fulfilment of requirements

for the degree of

Master of Science

April, 2011

Your file Votre référence
ISBN: 978-0-494-82825-0
Our file Notre référence
ISBN: 978-0-494-82825-0

ABSTRACT

DESIGNING EXPERIMENTS TO ASSESS THE SPACE-TIME DYNAMICS OF PLANT DISEASES

Daria Martchenko
University of Guelph, 2011

Advisors:
Dr. R. Deardon and Dr. P. McNicholas

Infectious diseases of plants can cause havoc both economically and environmentally. In order to control such disease it is desirable to understand the dynamics, which are generally spatio-temporal in nature, of the disease spread. In some situations experiments may be carried out to assess such dynamics. However, little work has been done exploring how best to design such experiments. Using a simple spatial Individual Level Model (ILM) we explore three spatial layouts (grid, Gaussian and deterministic). Employing Markov chain Monte Carlo (MCMC) methods within a Bayesian framework we investigate the estimation of disease spread model parameters under the different experimental layouts and spatio-temporal restrictions.

Table of Contents

List of Figures

Chapter 1

Introduction

Infectious diseases are one of the main factors affecting the wellbeing of humanity, both directly through human diseases, and indirectly through the diseases of agriculturally and economically important species. In order to control such diseases it is important to understand the spatio-temporal dynamics of their spread. Mathematical and statistical modeling has been gaining popularity as an analysis tool in this research area.

Models can be fitted at the individual level, where there are four states possible for each individual - susceptible (S), exposed (E), infectious (I) and removed (R). The models are usually used to analyze observational data (O'Neill, 2010), but can help identify the optimal design for a future experiment, for example on crops. Due to time and monetary constraints, it is important to have an experimental design that provides precise and accurate estimates of model parameters. This question of spatial layout and experiment duration over which spatial data should collected in order to understand the spatio-temporal dynamics of the disease spread is addressed in Chapter 2, a manuscript to be submitted to the journal of *Spatial and Spatio-temporal Epidemiology*. A simplified individual level model with only two possible states for each individual - suscepti-

ble and infected is employed. An epidemic is simulated in a population of one hundred individuals distributed in space according to three spatial layouts (grid, Gaussian and deterministic). Two scenarios are analyzed - one with unrestricted experimental area and duration, and one scenario under which both experimental area and duration are limited. Markov chain Monte Carlo algorithm (MCMC), within a Bayesian framework, is then used to fit a model to simulated epidemic data and estimate model parameters as if they are unknown. The layouts are compared on the basis of posterior precision and accuracy of those parameters. The findings from this study are described further in Chapter 2.

Chapter 2

Designing Experiments to Assess the Space-Time Dynamics of Plant Diseases

2.1 Introduction

Infectious diseases of crops, and other plants, can have dramatic economic and environmental consequences. In order to control such disease it is desirable to understand the dynamics of the disease spread. Mathematical and statistical modeling of infectious diseases has become a popular way of addressing this topic.

O'Neill (2010) provides a review of disease transmission models and their use for the analysis of observational data and decision-making. Such models can be developed to predict disease spread at an individual level (an individual could be a group, such as household or school, that is considered a unit for the purposes of the model). The individual then generally moves through four possible states - susceptible (S), exposed

(E), infectious (I) and removed (R). Models can be simplified by including only two or three states.

The models discussed by O'Neill (2010) can be used for observational data on human, animal and plant diseases. Due to ethical reasons, experiments on humans are not possible, and they can be difficult to implement on animals. Plant epidemiology has greater possibilities for experimental model testing and validation on real data. Experiments may also be carried out to assess the spatio-temporal dynamics of disease spread of plants. A discussion on classical experimental design in an agricultural setting is given by Mead et al. (2003). A number of interesting systematic designs have been suggested by Nelder (1962) for plant yield spacing experiments. In this paper we investigate a similar layout, but focus on epidemiological experiments.

In most cases plant pathologists study the spatial patterns of disease spread because they help explain the underlying mechanism of plant infection such as behaviour of carrier vectors (Hughes et al., 1997). In pioneer studies on plant epidemics, Bald (1937) found that tomato spotted wilt virus was transmitted to tomato plots by adult thrips from outside of the plot. The virus could only be acquired by thrips while they were nymphs, so adult thrips from outside of the plot could not infect the adult thrips who were already living on plants in the plot. That resulted in small clusters of infected tomatoes due to poor flight ability of thrips (Bald, 1937). Real and McElhany (1996) examined a static map of *Silene latifolia* infected with anther smut. Using join-count statistics and spatial autocorrelation they described the spatial structure in the plant and pathogen populations. Such analysis does not aide in the determination of the mechanism by which the disease had spread, since a number of different processes can result in the same spatial pattern (Real and McElhany, 1996).

However, spatial pattern itself can be an experimental treatment. Rodriguez-de Gon-

zalez et al. (1995) tested the effect of three initial infection patterns (uniform, random and segregated) on disease progression on plots of zucchini squash. A uniform infection pattern was found to result in the highest rate of disease progression while an aggregated pattern had the lowest rate. Spatial dynamics of disease spread can be investigated in manipulative experiments, where plots are subjected to different treatments, such as irrigation patterns (Hughes et al., 1997). Similarly to human and animal diseases, the models for plant diseases can be expanded to include networks. Jeger et al. (2007) review the implications of network model use for plant populations, such as farms or forest ecosystems. When fitting an infection model to real data the fit can be improved by inclusion of population heterogeneity in the the model. To account for overdispersion in their parametric model fit Soubeyrand et al. (2007) include frailties, which reflect the susceptibility of each individual to infection.

Conducting experiments on plants is costly and time-consuming. Prior to the experiment, it is important to which design would provide accurate and precise estimates of model parameters. Computer simulations allow for the development of such designs with low associated cost. Deardon et al. (2004) developed a simulation model of plant disease spread and investigated the effect of experimental layouts (complete and incomplete randomized block designs) on representation bias between treatment plots.

The problem we address here is not the identification of treatment effects in an experimental setting. Rather we seek to explore the usefulness of various experimental layouts when the purpose of the experiment is to identify the spatio-temporal dynamics of the disease spread itself. Here we present the results from a number of simulation studies that explore a number of spatial layouts of individuals within a single plot or field under varying area and time limitations. Models are fitted in a Bayesian MCMC framework (Gamerman and Lopes, 2006). Posterior precision and accuracy are the

basis for comparison between layouts.

2.2 Methods

The model being considered here is a simple spatial version of the Individual Level Model (ILM) for infectious diseases of Deardon et al. (2010). Here specifically, we consider an SI model. In such a model, an individual can be in one of two possible states at each point in discrete time: S - susceptible or I - infected. Once an individual has become infected, they remain in that state.

Under our spatial model, at a discrete time point t, a susceptible individual i has the probability $P(i,t)$ of being infected where:

$$P(i,t) = 1 - \exp\left[-\alpha \sum_{j \in I(t)} d_{ij}^{-\beta},\right]; \tag{2.1}$$

α is an infectivity parameter ($\alpha > 0$); β is the decay of the power-law dispersal kernel ($\beta > 0$), $\kappa(d_{ij}) = d_{ij}^{-\beta}$; d_{ij} is the Euclidean distance between a susceptible individual i and an infectious individual j; and $I(t)$ is the set of all infectious individuals at time t.

The likelihood function is then given by

$$f(D|\Theta) = \prod_{t=1}^{t_{max}} \prod_{i \in S_{t+1}} (1 - P_{it}) \prod_{i \in I_{t+1}} P_{it} \tag{2.2}$$

where S_{t+1} is the set of susceptible individuals, I_{t+1} is the set of newly infected individuals at time t, and Θ is the parameter vector, here $\Theta = (\alpha, \beta)$.

The study is conducted as follows. First, an epidemic is simulated in a population of up to 100 individuals. Individuals are placed in two-dimensional space according to one of three layouts: L_1, L_2 or L_3. These layouts are:

L_1 : *Grid Layout.* Individuals are positioned on a uniform square lattice with distance between positions in the x- and y-planes (δ_g).

L_2 : *Gaussian Layout.* X and Y coordinates of each individual are independently drawn from a Gaussian-Normal distribution, N(0, δ_n).

L_3 : *Circular Layout.* Individuals are placed on 'spikes' radiating from a centre-point at (0,0) with equal angles between each spike and the distance between individuals on each spike δ_c.

Examples of L_1, L_2 and L_3 are shown in Figures 1(a), (b) and (c) respectively.

The grid layout L_1 might be thought of as the default layout. The Gaussian layout would not be practical in implementation but is hypothesized to provide more precise and accurate estimates of model parameters. The circle layout L_3 is chosen because it in some sense deterministically resembles the Gaussian layout (a decreasing concentration of individuals from the center out) but would be much easier to implement.

Simulations are run under two scenarios. Under the first scenario, the experimental area and length of time that the epidemic is allowed to run for are restricted (R). These restrictions are set to be 20×20 square units for the area and 20 time units for duration. So, under the *restricted scenario*, if not all are infected, the experimental duration is 20 time units. Under the second scenario, there are no restrictions on the area and the simulation is run until all individuals become infected. Experimental duration is determined by the time it takes for all individuals to become infected. We refer to that as the *unrestricted scenario.*

For the first two layouts the spread of individuals is controlled by a single parameter. For the grid layout the distance between individuals, δ_g, is varied from 0.25 to 2 in increments of 0.25. The grid layout then falls under the restricted scenario area for

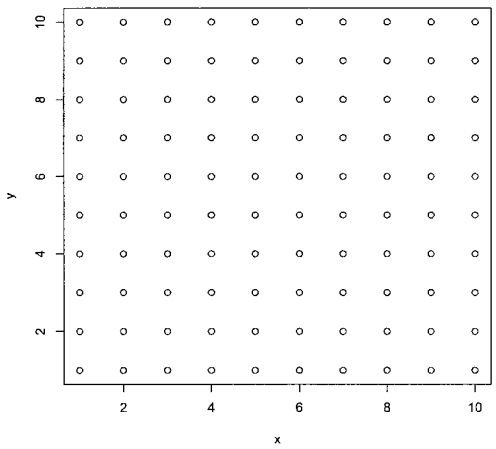

(a) Grid layout with δ_g=1.0.

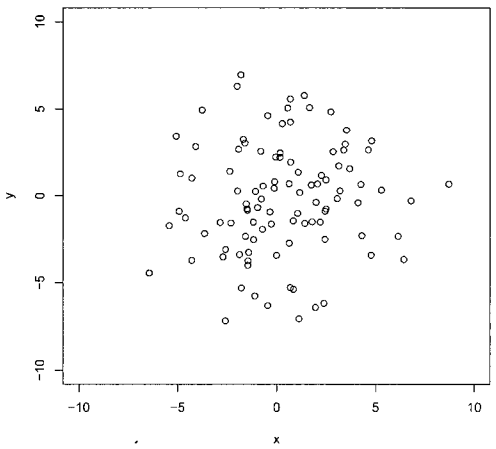

(b) Gaussian layout with δ_n=9.

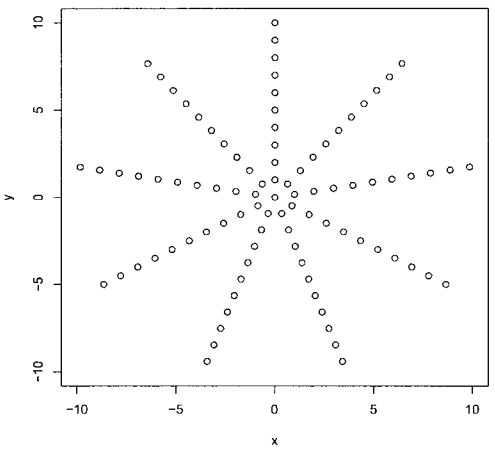

(c) Circular layout with 9 'spikes' and δ_c=1.0.

Figure 2.1: Typical experimental layouts.

all values of δ_g. For all grid layout simulations the epidemic took less than 20 time units, so the restricted scenario conditions are naturally met by the grid layout. For the Gaussian layout, the variance of the Gaussian, δ_n, is varied from 1 to 42.25 (1^2 to 6.5^2). For the deterministic layout two parameters are needed - the number of 'spikes' and the distance between the individuals on each 'spike' δ_c.

Values of α=1.0 and β=3.0 are used to simulate an epidemic in a population of 100 individuals. To start an epidemic, an individual is infected randomly. Then, at each subsequent time point each susceptible individual is infected with probability given by (2.1). Each simulation is repeated 10 times. Data generated from the various experiments are then analyzed. α and β are estimated as if they are unknown, using Markov chain Monte Carlo (MCMC) methods under a Bayesian framework. A Metropolis-Hastings MCMC algorithm is used with random walk proposals which are tuned to produce acceptable mixing. Positive half-normal priors are placed on α and β with variance 5000. In all cases, results from 9,000 iterations (10,000 iterations with a burn-in period of 1,000) of the algorithm are used to calculate the posterior precision (inverse of the variance), mean, bias and mean square error (MSE) for α and β. Convergence of MCMC is ascertained visually. Here the posterior precision and MSE of α and β are used to compare the experimental layouts.

2.3 Results

2.3.1 Grid layout (L_1)

The posterior MSE of α tends to increase as δ_g increases (Figure 2.2a). The posterior MSE of β decreases as δ_g increases from 0.25 to 0.75 and then appears to increase slightly as δ_g increases further. (Figure 2.2b).

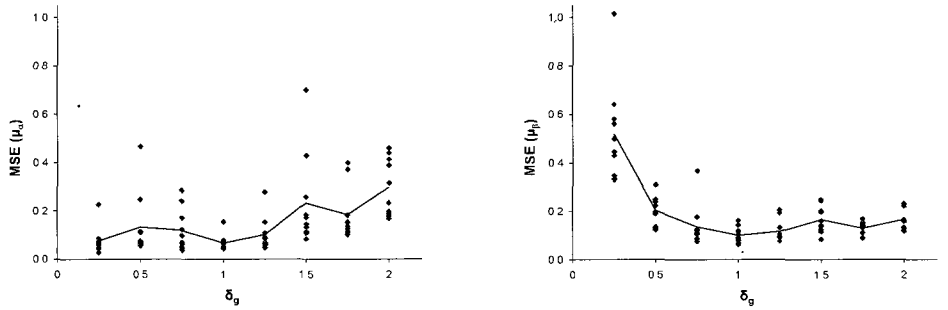

(a) MSE of posterior α values vs. distance between individuals (δ_g) (dots show MSE from individual simulations, line shows mean MSE).

(b) MSE of posterior β values vs. distance between individuals (δ_g) (dots show MSE from individual simulations, line shows mean MSE).

Figure 2.2: Grid layout L_1.

2.3.2 Gaussian layout (L_2).

Unrestricted scenario

The average posterior MSE of α is approximately constant at 0.10, with slight increases to 0.11 when δ_n is 4 and to 0.18 when δ_n is 25. The posterior MSE of β tends to decrease while δ_n increases to 12.25 and then plateaus (Fig. 2.3b). The variability of the posterior MSE of β is noticeably higher for the lower values of δ_n tested.

Restricted scenario

The range of posterior MSE for both α and β stays roughly the same under the restricted scenario as it is under the unrestricted scenario (Fig. 2.4). The mean of the posterior MSE of α follows a similar pattern under both scenarios. It is fairly constant around 0.1 with slight increases at δ_n of 9 and 12.25. Similar to the unrestricted scenario, the posterior MSE of β tends to decrease while δ_n increases to 25 (Fig. 2.4b) and then stays below 0.1.

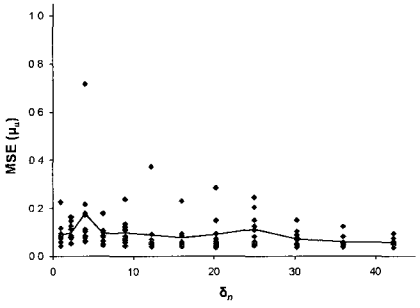

(a) MSE of posterior α values vs. δ_n with coordinates of individuals distributed as Normal $(0, \delta_n)$ (dots show MSE from individual simulations, line shows mean MSE).

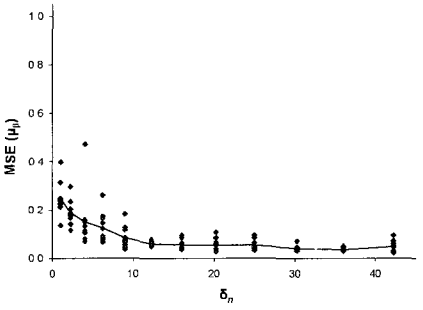

(b) MSE of posterior β values vs. δ_n with coordinates of individuals distributed as Normal $(0, \delta_n)$ (dots show MSE from individual simulations, line shows mean MSE).

Figure 2.3: Gaussian layout L_2 under the unrestricted scenario.

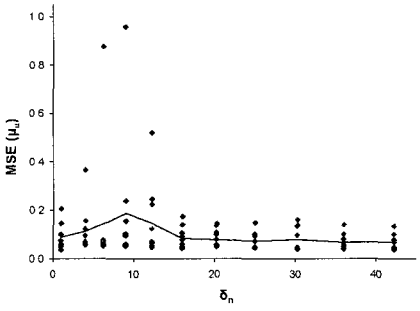

(a) MSE of posterior α values vs. δ_n with coordinates of individuals distributed as Normal $(0, \delta_n)$ (dots show MSE from individual simulations, line shows mean MSE).

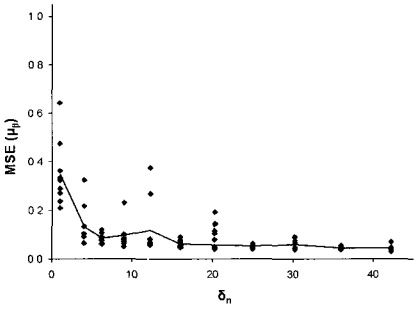

(b) MSE of posterior β values vs. δ_n with coordinates of individuals distributed as Normal $(0, \delta_n)$ (dots show MSE from individual simulations, line shows mean MSE).

Figure 2.4: Gaussian layout L_2 under the restricted scenario.

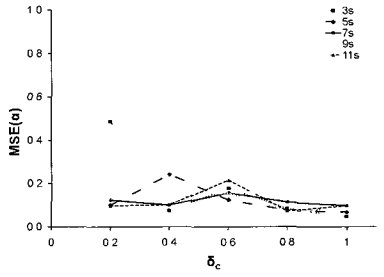

(a) Average MSE of posterior α values vs. δ_c with individuals distributed on circular layouts with 3,5,7,9 and 11 'spikes'.

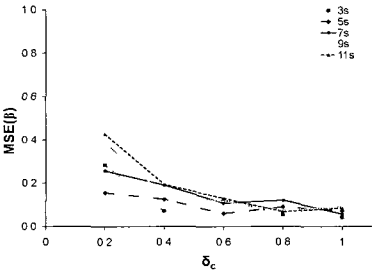

(b) Average MSE of posterior β values vs. δ_c with individuals distributed on circular layouts with 3,5,7,9 and 11 'spikes'.

Figure 2.5: Circular layout L_3 under the unrestricted scenario.

2.3.3 Circular layout (L_3)

Unrestricted scenario

The posterior MSE of β for deterministic layouts with 3 to 11 'spikes' generally decreases as the distance between individuals on each 'spike' increases (Fig. 2.5b). There is a slight increase in the posterior MSE of β when δ_c goes from 0.8 to 1 for layouts with 9 and 11 'spikes'. The posterior MSE of α is highest when δ_c is 0.6 for designs with 7, 9 and 11 'spikes' (Fig. 2.5a). The highest value of the posterior MSE of α occurs when δ_c is 0.2 on the 3 'spike' layout.

Restricted scenario

The area restriction only affects the 3 'spike' layout with δ_c from 0.4 to 1, the 5 'spike' layout with δ_c from 0.6 to 1, and the 7 'spike' layout with δ_c from 0.8 to 1. Layouts with 9 and 11 'spikes' remain the same. Reduction in area results in higher posterior MSE of α values for affected layouts (Figure 2.6a). This effect is greater for the posterior MSE of β, with values increasing from below 0.1 to above 0.2 when δ_c is 1 for layouts

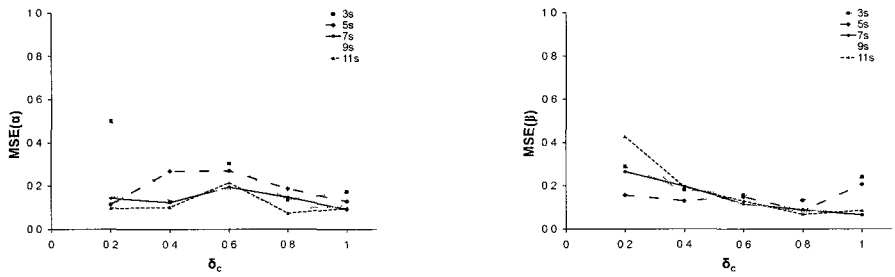

(a) Average MSE of posterior α values vs. δ_c with individuals distributed on circular layouts with 3,5,7,9 and 11 'spikes'.

(b) Average MSE of posterior β values vs. δ_c with individuals distributed on circular layouts with 3,5,7,9 and 11 'spikes'.

Figure 2.6: Circular layout L_3 under the restricted scenario.

with 3 and 5 'spikes'.

Example: 11 'spikes'

A spatial design with 11 'spikes' naturally falls under the restricted scenario, so only one set of simulations is needed. The posterior precision of α varies from 0.03 to 0.6 and does not show any clear trend (Figure 2.7a). The posterior precision of β tends to decrease as δ_c increases (Figure 2.7b).

2.3.4 Comparison

To provide an additional means of comparison between the three layouts, the posterior MSE and precision of α and β are plotted against the experimental area for the restricted scenario (Figures 2.8 to 2.11). Experimental area is the area of a rectangle limited by the individuals located furthest from the center. For example, for the grid layout, δ_g of 0.5 corresponds to an experimental area of 20.25 units squared. For the circular restricted layout with 3 'spikes' and δ_c of 0.6 the experimental area is 302.10 units

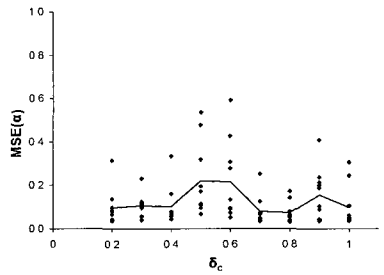

(a) Average MSE of posterior α values vs. δ_c (dots show MSE from individual simulations, line shows mean MSE).

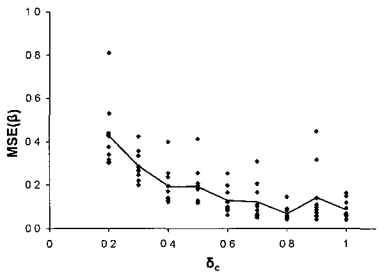

(b) Average MSE of posterior β values vs. δ_c (dots show MSE from individual simulations, line shows mean MSE).

Figure 2.7: Circular layout L_3 with 11 'spikes'.

squared. The experimental area for the Gaussian layout changes for every simulation.

For experimental areas less than 50 square units the posterior MSE of α is similar between the three layouts (Figure 2.8). For areas from 50 to 130 the posterior MSE of α is highest for the circular layout. For areas greater than 130 the posterior MSE of α is higher for the grid layout. The posterior MSE of β is similar between the three layouts with the exception of areas less than 130 square units (Figure 2.9). The posterior MSE of β is lowest for the grid layout and highest for the Gaussian layout.

When the experimental area is less than 50, the posterior precision of α is similar for all three layouts (Figure 2.10). For experimental areas between 50 and 130 square units the posterior precision of α is highest for the grid layout and lowest for the circular layout. For areas above 130 square units the circular and Gaussian layouts outperform the grid layout in terms of the posterior precision of α. The grid layout provides the highest posterior precision of β among the three layouts (Figure 2.11). For areas above 130 square units the posterior precision of β is highest for the circular layout followed by the Gaussian layout.

Figure 2.8: MSE of posterior α values vs. experimental area for all layouts under the restricted scenario.

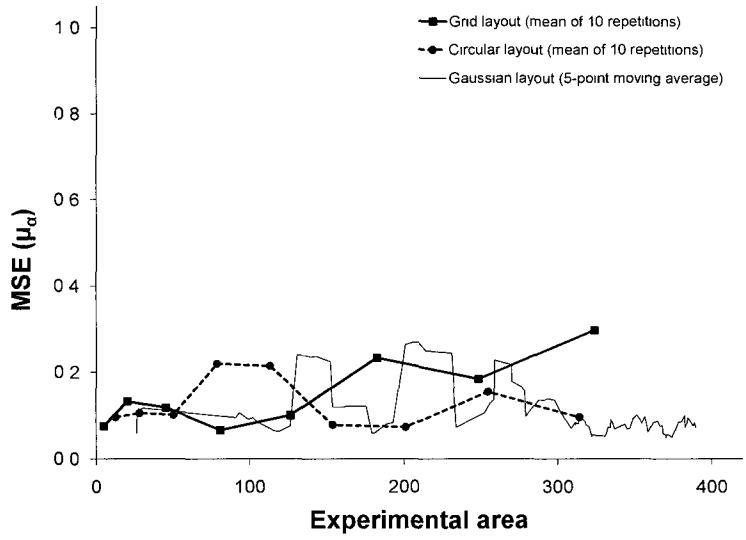

2.4 Discussion

The results of this study imply there is little to choose overall between the three layouts when fitting an SI ILM to spatial disease progress data. We can see that the choice of design parameters for particular layouts can be important. However, even this is complicated by the fact that improvements in the posterior MSE for one parameter are not necessarily met by an improvement in the posterior MSE for the other parameter. For example, under the grid layout we see that the posterior MSE of α tends to be lowest and the posterior MSE of β tends to be highest under small values of δ_g (Figure 2.2). However, the same results show that a choice of δ_g=1 leads to a fairly low posterior MSE values in terms of both model parameters. It may be that the approach taken in this paper could be used to optimize designs within the context of particular layouts, or

Figure 2.9: MSE of posterior β values vs. experimental area for all layouts under the restricted scenario.

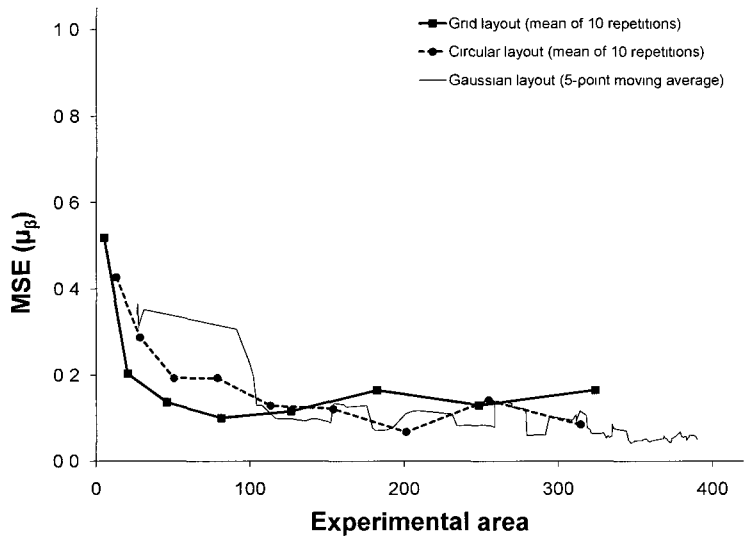

at least avoid very poor designs, when a priori knowledge about the model parameters is available.

Due to the area restriction in the circular layout fewer individuals were included in the experiment under the restricted scenario. This appears to have resulted in an increase in the posterior MSE of α and β for designs with 3, 5, and 7 'spikes'. The number of individuals in a plot is an important factor for the circular layout. The designs under layouts L_1 and L_2 were not observed with smaller populations because, in the case of the grid layout, even under the restricted scenario, 100 individuals were always included, and for the Gaussian layout individuals were sampled with replacement. Unlimited area and experimental duration do not result in lower posterior MSE for α and β for the Gaussian layout. The variability of the posterior MSE is also similar between the two scenarios for that layout.

Figure 2.10: Posterior precision of α vs. experimental area for all layouts under the restricted scenario.

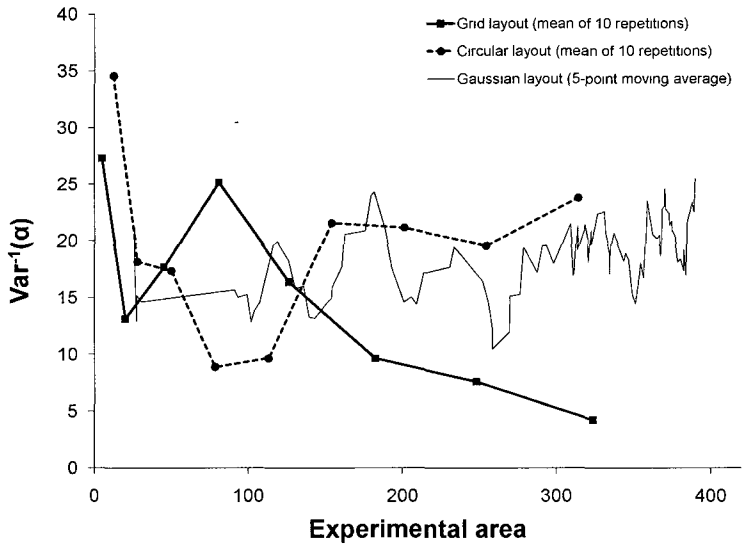

The tested layouts do have some limitations with respect to implementation. If the discussed model is implemented in a physical experiment, the Gaussian layout is not expected to achieve the same results as in simulation. Under simulation it allows for plants to be placed in on top of each other, which would obviously not be possible in reality. The Gaussian layout is used here for exploratory and comparison purposes. For an experiment with available area of less than 130 square units the recommended layout is the grid with distance between individuals ranging from 0.75 to 1. If an area greater than 130 square units is available, the circular layout provides higher posterior precision and lower posterior MSE for α and β estimates.

The scenarios tested here ignore some biological factors that could, in some circumstances, have an effect on results. For example, in a real-life experiment it may be that a plant's disease resistance could be reduced due to competition for resources with

Figure 2.11: Posterior precision of β vs. experimental area for all layouts under the restricted scenario.

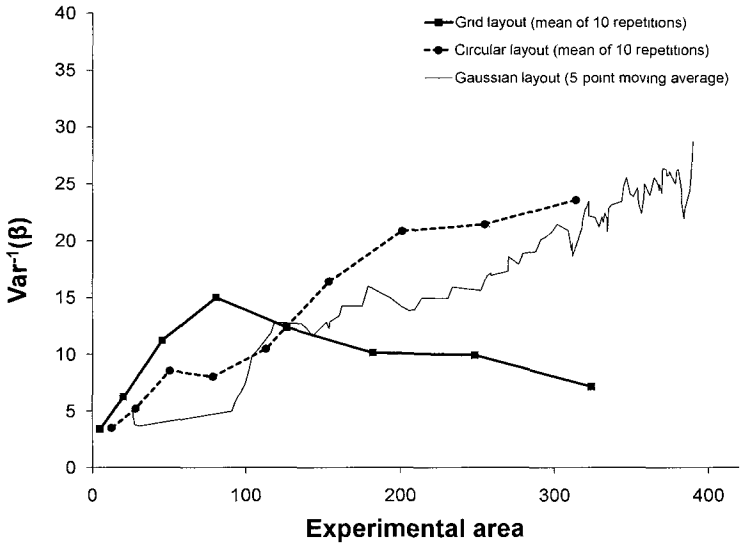

neighbours in close proximity. Experimental designs suggested here would also not be applicable to some plant diseases that result in a 'simple interest' type of epidemic (Hughes et al., 1997) where the pressure of infection is coming mainly from outside of the plot and transmission rate between the individuals is very low. Simple modifications of the ILM used here, however, could allow for external infection pressure.

To make the experiment more realistic, heterogeneity could be introduced into the model. This would incorporate environmental conditions into the model, for example richer soil and, therefore more preferable conditions for some plants, in one part of the field. Another possibility is the addition of a directional variable that takes account environmental factors that affect the spread of infection, such as wind direction or field grade. Another possible layout to be tested is a clustered pattern, where plants would be planted in groups with a certain distance between them. In an experiment by

Rodriguez-de Gonzalez et al. (1995) slower rate of disease progression was found for an aggregated infection pattern. It would be of interest to see if such a design could improve parameter estimation.

Acknowledgements

This work was carried out by Martchenko as part of her M.Sc. studies with Deardon and McNicholas. It was funded in part by the Natural Sciences and Engineering Research Council (NSERC) of Canada Discovery Grants Program. This work was also made possible through the use of computing facilities funded in part by the Canada Foundation for Innovation (CFI) and the Natural Sciences and Engineering Research Council of Canada (NSERC), courtesy of Profs. Monica Cojocaru and Hermann Josef Eberl. The equipment was provided by SGI.

Bibliography

Bald, J.G., 1937. Investigations on spotted wilt of tomatoes iii: Infection of field plots. Bulletin Australian Council for Scientific and Industrial Research 106, 32.

Deardon, R., Brooks, S.P., Grenfell, B.T., Keeling, M.J., Tildesley, M.J., Savill, N.J., Shaw, D.J., Woolhouse, M.E.J., 2010. Inference for individual-level models of infectious diseases in large populations. Statistica Sinica 20, 239–261.

Deardon, R., Gilmour, S.G., Butler, N.A., Phelps, K., Kennedy, R., 2004. A method for ascertaining and controlling representation bias in field trials for airborne plant pathogens. Journal of Applied Statistics 31, 329–343.

Gamerman, D., Lopes, H.F., 2006. Markov Chain Monte Carlo: Stochastic Simulation for Bayesian Inference. Chapman and Hall/CRC.

Rodriguez-de Gonzalez, P., Cho, J.J., Ullman, D., Nelson, S.C., 1995. Effect of different initial spatial patterns of zucchini yellow mosaic virus (zymv) on the spatial and temporal disease spread in zucchini squash (Abstract). Phytopathology 85, 1122.

Hughes, G., McRoberts, N., Madden, L.V., Nelson, Scot Carter, E.M., 1997. Validating mathematical models of plant-disease progress in space and time. Mathematical Medicine and Biology 14, 85–112.

Jeger, M.J., Pautasso, M., Holdenrieder, O., Shaw, M.W., 2007. Modelling disease spread and control in networks: implications for plant sciences. New Phytologist 174, 279–297.

Mead, R., Curnow, R.N., Hasted, A.M., 2003. Statistical methods in agriculture and experimental biology. Chapman & Hall/CRC.

Nelder, J.A., 1962. New kinds of systematic designs for spacing experiments. Biometrics 18, pp. 283–307.

O'Neill, P.D., 2010. Introduction and snapshot review: Relating infectious disease transmission models to data. Statistics in Medicine 29, 2069–2077.

Real, L.A., McElhany, P., 1996. Spatial pattern and process in plant-pathogen interactions. Ecology 77, pp. 1011–1025.

Soubeyrand, S., Sache, I., Lannou, C., Chadoeuf, J., 2007. A frailty model to assess plant disease spread from individual count data. Journal of Data Science 5, 68–81.

Appendix A

Posterior Precision Graphs

The appendix includes graphs of the posterior precision of α and β for the three layouts - grid, Gaussian and circular.

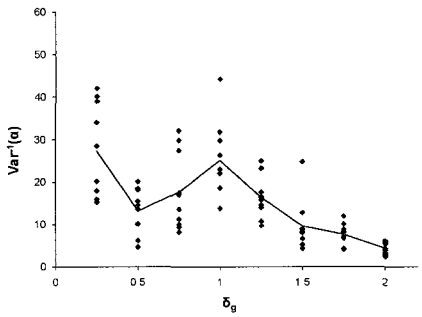

(a) Posterior precision of α vs. distance between individuals (δ_g)) (dots show the posterior precision from individual simulations, line shows mean posterior precision).

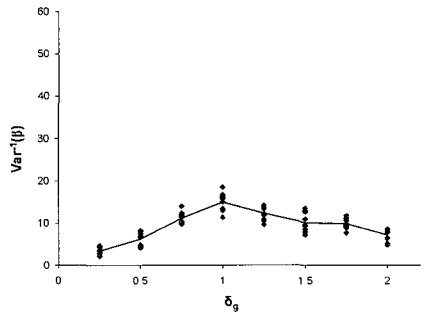

(b) Posterior precision of β vs. distance between individuals (δ_g)) (dots show the posterior precision from individual simulations, line shows mean posterior precision).

Figure A.1: Grid layout L_1.

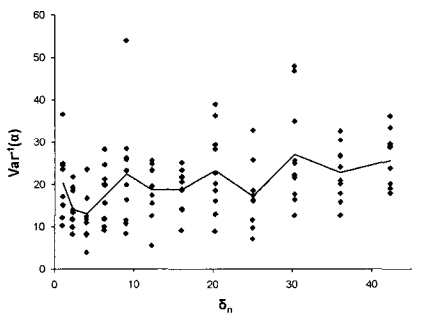

(a) Posterior precision of α vs. δ_n with coordinates of individuals distributed as Normal (0, δ_n) (dots show the posterior precision from individual simulations, line shows mean posterior precision).

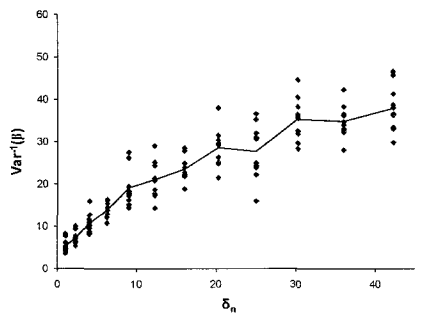

(b) Posterior precision of β vs. δ_n with coordinates of individuals distributed as Normal (0, δ_n) (dots show the posterior precision from individual simulations, line shows mean posterior precision).

Figure A.2: Gaussian layout L_2 under the unrestricted scenario.

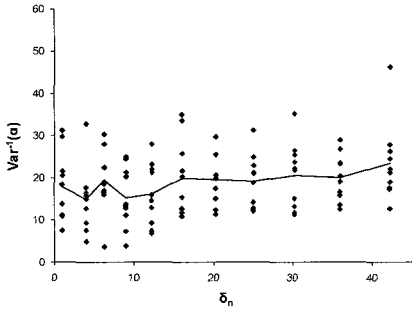

(a) Posterior precision of α vs. δ_n with coordinates of individuals distributed as Normal (0, δ_n) (dots show the posterior precision from individual simulations, line shows mean posterior precision).

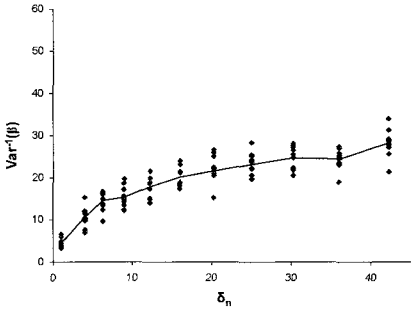

(b) Posterior precision of β vs. δ_n with coordinates of individuals distributed as Normal (0, δ_n) (dots show the posterior precision from individual simulations, line shows mean posterior precision).

Figure A.3: Gaussian layout L_2 under the restricted scenario.

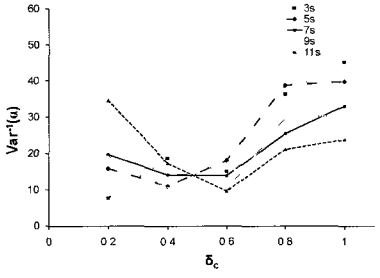

(a) Average posterior precision of α vs. δ_c with individuals distributed on circular layouts with 3,5,7,9 and 11 'spikes'.

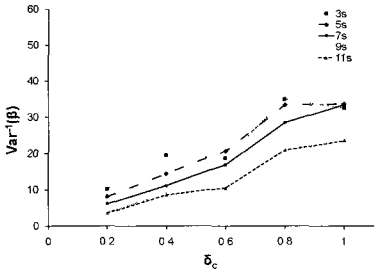

(b) Average posterior precision of β vs. δ_c with individuals distributed on circular layouts with 3,5,7,9 and 11 'spikes'.

Figure A.4: Circular layout L_3 under the unrestricted scenario.

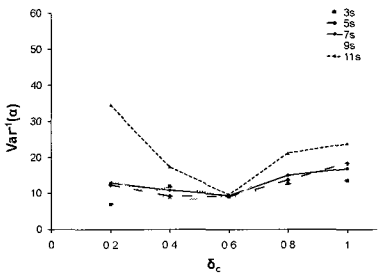

(a) Average posterior precision of α vs. δ_c with individuals distributed on circular layouts with 3,5,7,9 and 11 'spikes'.

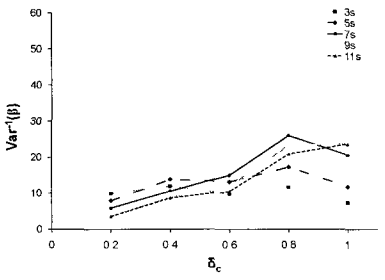

(b) Average posterior precision of β vs. δ_c with individuals distributed on circular layouts with 3,5,7,9 and 11 'spikes'.

. Figure A.5: Circular layout L_3 under the restricted scenario.

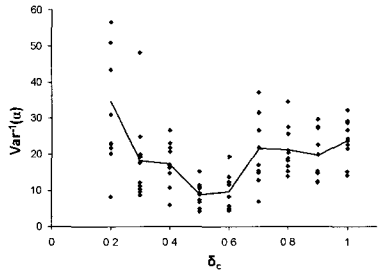

(a) Average posterior precision of α vs. δ_c (dots show the posterior precision from individual simulations, line shows mean posterior precision).

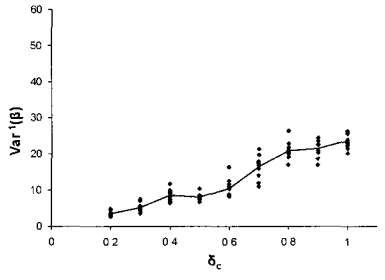

(b) Average posterior precision of β vs. δ_c (dots show the posterior precision from individual simulations, line shows mean posterior precision).

Figure A.6: Circular layout L_3 with 11 'spikes'.